Archives of Biochemistry and Biophysics 772 (2025) 110555

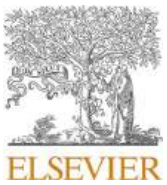

Contents lists available at ScienceDirect

Archives of Biochemistry and Biophysics

journal homepage: www.elsevier.com/locate/yabbi

The molecular mechanism of $P2Y_1$ receptor activation by inorganic polyphosphates

Khondamir R. Rustamov [a], Albert R. Makhmudov [a,e], Fozila R. Ikromova [a,c], Ekaterina A. Vetrova [b], Andrey Y. Vinokurov [b], Jamoliddin I. Razzokov [f], Andrey Y. Abramov [b,d], Artyom Y. Baev [a,b,c,*]

[a] Laboratory of Experimental Biophysics, Centre for Advanced Technologies, Tashkent, Uzbekistan
[b] Cell Physiology and Pathology Laboratory, Orel State University, Orel, 302026, Russia
[c] Department of Biophysics, Faculty of Biology, National University of Uzbekistan, Tashkent, Uzbekistan
[d] Department of Clinical and Movement Neurosciences, UCL Queen Square Institute of Neurology, Queen Square, London, WC1N 3BG, UK
[e] Department of Chemistry, KU Leuven, Celestijnenlaan 200f, Box 2404, 3001, Leuven, Belgium
[f] Institute of Fundamental and Applied Research, National Research University TIIAME, Kori Niyoziy 39, 100000, Tashkent, Uzbekistan

ARTICLE INFO

Keywords:
Inorganic polyphosphate
$P2Y_1R$
Purinoreceptors
Molecular dynamics

ABSTRACT

$P2Y_1$ receptors ($P2Y_1Rs$) are metabotropic purinoreceptors that can be activated primarily by ADP and, to a lesser extent, by ATP. Recently it was demonstrated that $P2Y_1R$ can be activated by inorganic polyphosphates (polyPs) – molecules, composed solely of orthophosphate residues and lacking a purine part. Although numerous studies have demonstrated that extracellular polyP can transmit signals to neighboring cells via activation of $P2Y_1R$, the precise molecular mechanisms underlying the activation of $P2Y_1R$ by polyP are still unclear. Here, using all-atom molecular dynamics simulations, we demonstrate that polyP binding to the inactive $P2Y_1R$ induces conformational changes of the receptor, causing its transition into the active state. Binding of polyP-14 to $P2Y_1R$ disrupts the interaction between Asp204 and Arg310 residues, increases the solvent accessible surface area (SASA) of receptor's binding pocket and induces bulk water influx into the receptor inner region. These processes induce conformational changes in the intracellular TM helices, leading to receptor activation similar to that observed in the presence of ADP. In agreement to *in silico* experiments, application of the same concentrations of polyP and ADP induced calcium signal in skin fibroblasts with similar shape and amplitude. Thus, our findings establish that polyP molecules can bind to and activate $P2Y_1$ purinoreceptor by molecular mechanism similar to those of its natural ligand ADP. We also propose the hypothesis that interaction of pyrophosphate part of ADP or polyphosphate with certain amino acids is a key event in $P2Y_1R$ activation.

1. Introduction

Inorganic polyphosphates (polyPs) are homopolymers composed of orthophosphates residues, linked together by phosphonanhydride bonds like in ATP molecule [1]. PolyP is present in all living organisms including all types of mammalian cells and its metabolism is tightly coupled to energy conversion system of the cell [2–6]. Many cellular metabolites, such as glutamate, succinate, ATP etc., while playing their own role inside the cell, when excreted extracellularly could spread signals to neighboring cells by interacting with specialized cell receptors. PolyP can be released by activated platelets, mast cells and basophils and take part in coagulation, migration, inflammation, wound healing, and differentiation processes [7–9]. In the brain polyP can be released by astrocytes and facilitate physiological communication between them [10–12]. Moreover, release of polyP from astrocytes was also observed during pathological conditions such as hypoxia [12], in amyotrophic lateral sclerosis (ALS) and frontotemporal dementia (FTD) [13]. However, while in glutamate excitotoxicity extracellular polyP has been shown to be protective by modulating glutamate receptors activity [14], release of polyP during ALS/FTD caused toxicity to neighboring motoneurons, via unknown mechanisms [13]. Based on the current data, extracellular polyP can interact with metabotropic $P2Y_1$ receptor ($P2Y_1R$). Activation of $P2Y_1R$ by polyP in astrocytes leads to the activation of phospholipase C and inositol 1,4,5-trisphosphate (IP_3)

* Corresponding author. 3A, Talabalar shaharchasi, Tashkent, 100174, Uzbekistan.
E-mail address: baev.a.yu@gmail.com (A.Y. Baev).

https://doi.org/10.1016/j.abb.2025.110555
Received 11 March 2025; Received in revised form 7 July 2025; Accepted 17 July 2025
Available online 18 July 2025

dependent calcium release from endoplasmic reticulum (ER). Binding of extracellular polyP to $P2Y_1R$ and concomitant increase of intracellular calcium concentration causes fusion of vesicles containing Vesicular Nucleotide Transporter (VNUT), containing polyP, with the astrocyte's plasma membrane and release of polyP into the intercellular space through exocytosis [10,12]. Interaction of polyP with P2Y1R was also observed in HUVEC and vascular endothelial cells [15–17]. However, there were also observations, showing that treatment of SaOS-2 cells for 30–60 min with exogenous polyP caused release of matrix vesicles, which contained both alkaline phosphatase (ALP) and adenylate kinase (AK) into the extracellular space [18,19]. The authors demonstrated that treatment of SaOS-2 cells with polyP, accompanied by the release of ALP and AK, led to an increase of extracellular ATP and ADP via unknown mechanism [18,19]. Based on these observations, some groups suggested that the effect of polyP on $P2Y_1R$ is not direct, but mediated by the formation of ATP and ADP in the intercellular space [20]. In order to clarify these aspects, we explore the mechanisms of $P2Y_1R$ activation by polyP and compare its effects with those of ADP, which has been proven as the native ligand of $P2Y_1R$.

$P2Y_1R$ are metabotropic G protein coupled receptors (GPCRs), activated by ADP and ATP (ADP – full agonist, ATP – partial agonist). Ligand binding leads to the formation of an active conformation of $P2Y_1R$, involving the recruitment and activation of G_S-proteins. Activation of all GPCRs is coupled with the formation of a continuous internal water pathway [21]. Moreover, recent research showed that activation of $P2Y_1R$ by ADP is coupled with the breakage of the ionic lock between $Aspartate^{204}$ and $Arginine^{310}$, while selective $P2Y_1R$ inhibitors MRS2500 and BPTU stabilized this ionic lock even at the presence of ADP [22]. ADP-dependent breakage of the ionic lock led to an increase of solvent accessible surface area (SASA) of the $P2Y_1R$, inducing a water influx into the binding pocket. These events forced transmembrane domains 3, 6 and 7 (TM3, TM6, and TM7) to change their position, which opens up an intracellular pocket to which Gα-subunit can bind [22].

Here, we used all-atom molecular dynamics (MD) simulations to investigate the mechanisms of $P2Y_1R$ activation in the presence of polyP and ADP. Moreover, we compared the efficacy of these two ligands to activate $P2Y_1R$ in live cell experiments with primary fibroblasts.

2. Materials and methods

2.1. Modelling the $P2Y_1R$ structure in inactive state

There are two X-ray (4XNW, 4XNV) and one cryo-EM (7XXH) structures of human $P2Y_1R$ in the PDB database [23]. The first two structures are bound to $P2Y_1R$ antagonists - MRS2500 and BPTU, the latter one is with the agonist - MeSADP. For our study, we used the structure of the individual protein bound to MRS2500, as it is believed to better represent the inactive state. In comparison to MRS2500, BPTU interacts with the α-helices from the membrane side, which may result in a different conformational configuration and hence the BPTU-bound structure was not considered it in this work.

To crystallize the $P2Y_1R$ with MRS2500, authors inserted Rubredoxin fusion protein into the experimental structure instead of the intracellular loop 2 [23,24]. To address this issue, we reconstructed the $P2Y_1R$ in its inactive state by predicting its structure by means of AlphaFold2 [25]. As an input we used sequence of Rattus norvegicus (Rat) P2Y1R (Uniprot AD- P49651) For the masked template, we used MRS2500-bound $P2Y_1R$ structure (PDB: 4XNW). Five models of $P2Y_1R$ were generated and ranked them based on their pLDDT score [26]. Predicted models had high pLDDT score (supplementary figure 1 A) and maintained the fold of the template structure (supplementary figure 1 B, Table 1). The most accurate model was selected for our MD simulations.

While the AF2 prediction was guided by the MRS2500-bound 4XNW structure as a masked template, we acknowledge potential limitations inherent to template-based predictions. In particular, deviations may arise in flexible loop regions or in the packing of certain side chains, especially in areas not directly stabilized by the template. However, the predicted model showed a low RMSD (0.255 Å) relative to 4XNW and a high average pLDDT score (94.8), supporting the reliability of the overall fold. Furthermore, subsequent molecular dynamics simulations allowed for structural relaxation and refinement in a realistic membrane environment, mitigating potential local inaccuracies introduced by the prediction.

Table 1
Results of AlphaFold2 prediction.

Metric	Result
plDDT (full protein)	94.8
pTM	0.924
RMSD to 4XNW (Å)	0.255

2.2. ADP and polyP-14, 40, 60 docking to $P2Y_1R$

To study the binding poses of polyP of different lengths and compare them to ADP, we performed molecular docking using AutoDock Vina. First we constructed and optimized ligand geometries from SMILES representation using RDKit Python package and Open Babel as described in Ref. [27]. Afterwards, we prepared ligands 3D structures using AutoDock Vina scripts. We prepared the $P2Y_1R$ receptor structure taken from the previous step by assigning polar hydrogen atoms as well as partial charges as described in Ref. [28]. Prior to docking, we analyzed the approximate molecular dimensions of each ligand in its linear form: PolyP-14 was estimated to be 36.4 Å in length, while ADP measured 15.1 Å. However, when bound to the receptor, both ligands adopt a curved conformation within the binding pocket. From the docked structures, the spatial dimensions of the bound conformations were estimated to be approximately 11.3 × 11.7 × 3.2 Å for PolyP-14 and 8.5 × 8.7 × 3.6 Å for ADP, based on visual inspection and molecular modeling.

Accordingly, we defined the docking box size as 16 × 16 × 16 Å for PolyP-14 and 12 × 12 × 12 Å for ADP to ensure full coverage of the binding region and sufficient space to allow conformational flexibility during docking. The center of the docking box was positioned at the extracellular binding region of the receptor. The receptor structure was prepared by adding polar hydrogen atoms and partial charges according to standard AutoDock Vina protocols. The exhaustiveness parameter was set to 8 for all docking runs.

2.3. System setup

In order, to study the effects of PolyP-14 on $P2Y_1R$ using the MD simulations, we created 3 separate model system which include different states of receptor: 1) ligand-free, 2) ADP-bound, and 3) PolyP-14 bound states. All these systems were constructed on CHARMM-GUI web server [29]. The ligand-free (apo) state system was build using "Bilayer Builder" module, while ligand bound states were constructed using "High-Throughput Simulator" module. Receptor in all systems were placed in 106 1-palmitoyl-2-oleoyl-sn-glycero-3-phosphocholine (POPC) phospholipids, which were to simulate the lipid bilayer of cells. The force field parameters for ADP and PolyP were generated using CGenFF algorithm build in CHARMM-GUI web server. Further, all systems were solvated in TIP3 water model and neutralized with Na^+/Cl^- counterions at a 0.15 M concentration.

2.4. Molecular dynamics simulations

All simulations were carried out in GROMACS software [30] using CHARMM36 m forcefield [31]. In the first step, we minimized all three systems for 5000 steps using the steepest descent algorithm, then we followed a 6-step equilibration in the NVT ensemble. These constraints

were gradually decreased. After the equilibration procedure, we performed 3 replicas of 300 ns production runs in the NPT ensemble for all our systems using Partial Mesh Ewald (PME) methods to monitor long-range electrostatics as was described in Ref. [32]. For temperature coupling at 310.1 K Nose-Hoover thermostat was used. And the pressure was preserved with the help of Parrinello-Rahman barostat. All covalent bonds were constrained to the equilibrium length by the LINCS algorithm. In all replicas, the last frame of the equilibration run was used, but with different initial velocities.

2.5. Data analysis

We measured the RMSD of $P2Y_1R$ Cα atoms and calculated the minimal distance between salt bridge-forming residues over the course of the simulation using in-built tools in the GROMACS package [33]. To assess the distances between transmembrane (TM) helices, we defined the residues of the TM helices as described in Ref. [22] and calculated the minimum distances between them. Additionally, we used an in-house developed Python3 script to calculate the number of water molecules inside the receptor's transmembrane part. We defined the center of the membrane by measuring the center of mass of the phosphate head groups of the POPC molecules. Subsequently, we calculated the positions of all water molecules relative to the defined membrane center. Principal component analysis (PCA) of the transmembrane C_α atoms of the receptor was performed using the ScikitLearn Python library [34]. All structures were visualized using the ChimeraX and Discovery Studio software. The solvent-accessible surface area (SASA) of the protein was also calculated using the gmx sasa tool, with a probe radius of **0.14 nm**, corresponding to the approximate size of a water molecule.

For statistical analysis we used time-block averaging following with One Way ANOVA with post hoc Tukey test. For the block averaging method, we averaged every 20 ns of the simulation for the RMSD data — 300 ns of simulation resulted in 15 data points in each group. For the comparison of PCA analysis data, SASA, water molecules, and distances between transmembrane domains (TM), we used the last 100 ns of the simulations. For this type of data, averaging was performed every 10 ns −10 data points in each group.

2.6. Umbrella Sampling simulations

To thoroughly investigate the binding energy of polyP-14 and ADP to $P2Y_1R$, we conducted Umbrella Sampling (US) simulations as described in Ref. [35]. Initially, we extracted $P2Y_1R$ bound to PolyP-14 and ADP from the last frame of production run. To preserve structural stability during pulling, positional restraints were applied to the receptor backbone, lipid phosphate groups, and ligand heavy atoms. Then, we generated total starting positions for US simulation by pulling the ligands (ADP and PolyP-14) from receptor along the z-axis. Ligands were pulled out until the distance between the reaction coordinates reached 4 nm range by applying 1000 kJ*Mol*nm. Next, 40 umbrella windows with 0.1 nm range were extracted. Further, we performed 11 ns production simulation (1 ns of equilibration and 10 ns of sampling) for each umbrella window. To ensure adequate sampling and continuity along the reaction coordinate, we monitored the overlap of sampling distributions between adjacent windows. The potential of mean force (PMF) profiles for the binding of ADP and polyP-14 to P2Y1R were then calculated using the Weighted Histogram Analysis Method (WHAM) implemented in the GROMACS package.

2.7. Cell lines

Human skin fibroblasts, derived from healthy patients were used as a research object as was previously described in Ref. [36]. The number of passages did not exceed p20. DMEM (Biological Industries, Kibbutz Beit-Haemek, Israel), 10 % FBS (Biological Industries, Kibbutz Beit-Haemek, Israel) with 1 % GlutaMAX (Gibco, New York, USA) were applied for cultivation of skin fibroblasts. Cell cultures were maintained at 37 °C in a humidified atmosphere of 5 % CO2 and 95 % air. The confluence of cells during the studies was 40–50 %.

2.8. Fura-2 measurements

To assess the calcium signal, $[Ca^{2+}]_c$ was imaged using Fura-2 AM (Invitrogen). Skin fibroblasts were loaded with 5 μM Fura-2 am at room temperature for 30 min in Hanks Balanced Salt Solution composed (in mM): 156 NaCl, 3 KCl, 2 $MgSO_4$, 1.25 KH_2PO_4, 2 $CaCl_2$, 10 glucose and 10 HEPES, pH adjusted to 7.35 with NaOH. Fluorescence images were acquired (10 s interval) on an epifluorescence inverted microscope equipped with a 20x fluorite objective (excitation at 340 and 380 nm). The data presented as Fura-2 ratio (340nm/380 nm). The emitted light was reflected through a 515 nm long-pass filter to a CMYK camera (Retiga; QImaging) and digitized to 12-bit resolution (Cairn Research, UK). Experiments were repeated in three different days (3 cell passages) on 6 coverslips for both ADP and polyP experiments.

2.9. Statistical analysis

Statistical analysis (unpaired two sample *t*-test, p value set at 0.05) and curve fitting were performed using Origin 2021 (Microcal Software Inc., Northampton, MA) software. Results are expressed as means ± standard error of the mean (SEM).

3. Results

In previous reports it was shown that polyPs 14, 60, and 130 could increase intracellular calcium concentration by activating $P2Y_1R$ in the similar manner [10,14,15]. However as far as the size of these polyPs vary significantly, in the first series of experiments, we conducted molecular docking experiments to understand the binding pattern of different lengths polyPs with P2Y1R. The length of polyP in mammalian cells varies up to 100 residues [8]. Our experiments showed that polyP-14 perfectly enters the binding pocket of the receptor, similar to ADP (Fig. 1). However, the molecules of polyP-40 and -60 only partially entered the binding pocket of P2Y1R (Fig. 1).

Switching of the protein to the active state usually occurs when the ligand interacts with several key amino acids in the active center of the protein. All polyPs, fully or partially, interacted with the active center of the $P2Y_1R$ (Fig. 1). Thus, for further all-atom molecular dynamics (MD) simulations we used polyP-14. To investigate molecular mechanisms of $P2Y_1R$ activation by polyP we build three systems based on the crystal structure of P2Y1R (PDB: 4XNW): 1) in apo state - without ligand; 2) bound to ADP - its native ligand; 3) bound to PolyP-14 molecule.

After simulations we calculated Root Mean Square Deviation (RMSD) values for Cα atoms of receptors in different states for all simulation replicas. Our findings indicate that the receptor's conformation remains relatively stable during the simulation process. A shift in RMSD was observed across all three systems during the initial 40 ns of simulation. However, in the apo state, the receptor's RMSD subsequently stabilized and remained relatively constant throughout the remainder of the simulation (Fig. 2A–C and Sup. Fig. 2A and B). In contrast, the RMSD of $P2Y_1R$ in complex with ADP or polyP-14 continued to increase until the end of the simulation. Analysis of the final 100 ns of all trajectories revealed that binding of ADP and polyP-14 induced more pronounced RMSD changes compared to the apo state (Sup. Fig. 2A and B).

RMSD shows the structural distance between coordinates during the simulation; however, this parameter does not show the vector of the Cα atoms' coordinate shift. Thus, to understand the difference of Cα atoms dynamics between apo- and ligand bound states we performed the principal component analysis (PCA) test. The results of PCA test show that at the start of the simulation atoms of the $P2Y_1R$ from all three states

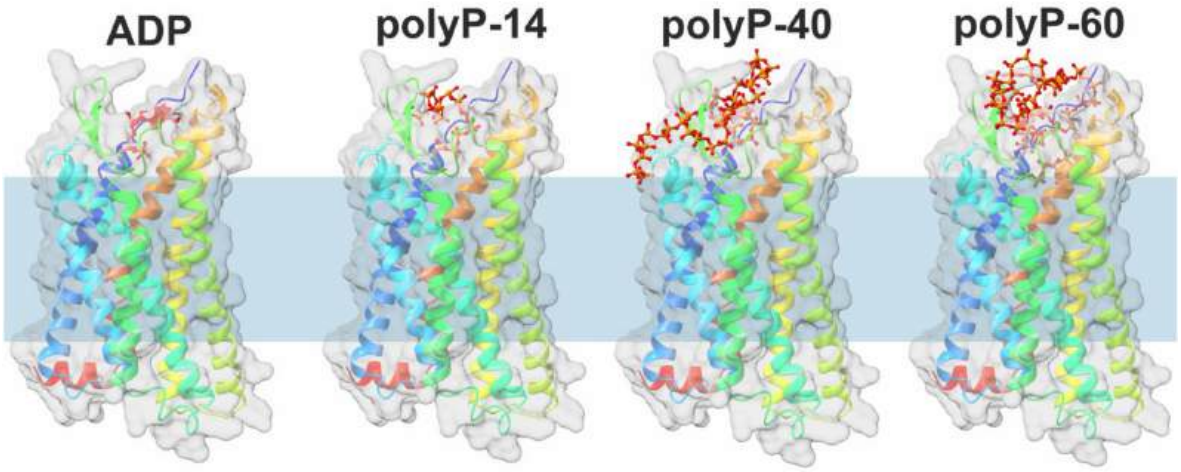

Fig. 1. Binding of ADP and polyPs of different lengths to P2Y1R.

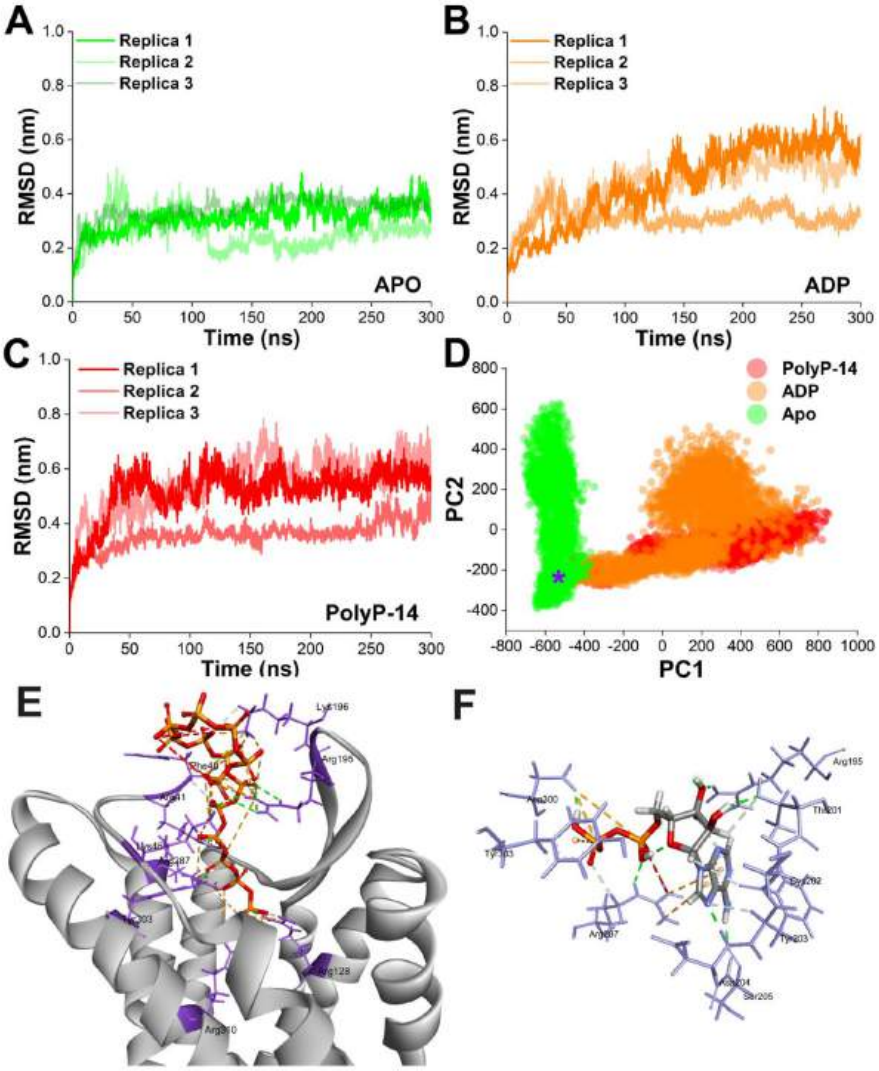

Fig. 2. Results of MD simulations. RMSD values of Cα atoms of 3 replica simulations for APO state (**A**), ADP bound state (**B**) and PolyP-14 bound state (**C**) of $P2Y_1R$. **D.** PCA of Cα atoms positions of $P2Y_1R$ in different states.

were at the same position (Fig. 2 D, indicated by star). During the simulation, the PolyP-14 and ADP-bound states exhibit similar shifts in conformational space, whereas the apo state of P2Y1R shows significantly different changes (Fig. 2 D, Sup. Fig. 2C).

To assess the interactions between ADP and polyP-14 with P2Y1R, we analyzed the final frames of the molecular dynamics simulations (300 ns). The results indicated that ADP interacts with several key amino acid residues (Fig. 2F–Table 2, highlighted in grey), including Arg195 [22,23,37], Leu44 [23] (and 8wjx[1]), Tyr203 [23,38], Arg287 [23,37,38] (and 8wjx), Ser (Thr) 205 [23,37,38] (and 8wjx), Asp204 [23,37] (and 8wjx). These residues have been previously reported to be critical for ADP (or 2MeSADP) binding and P2Y1R activation (Sup. Tables 2 and 3).

Notably, polyP-14 established interactions with an even broader set of functionally important residues, including Arg195 [22,23,37], Tyr203 [23,38], Arg287 [23,37,38] (and 8wjx), Lys46 [22,23], Arg (Lys) 41 [22], Arg310 [23,37,38] (and 8wjx), Arg128 [38] (and 8wjx), Tyr303 [22,23,38] (and 8wjx) (Fig. 2E–Table 2, highlighted in grey).

Thus, we showed that the binding of polyP-14 and ADP to an inactive form of P2Y1R causes a conformational shift of P2Y1R atoms during MD simulation in a similar way.

3.1. Binding of polyP and ADP to P2Y1R causes disruption of ionic lock between Asp204 and Arg310 and increase of SASA

Number of mutational and computational studies illustrated the essential role of Asp204 and Arg310 in $P2Y_1R$ activation [22]. It has been shown that the disruption of ionic lock between these residues leads to the activation of $P2Y_1R$, while the stabilization of the ionic lock between Asp204 and Arg310 is considered as the main mechanism of $P2Y_1R$ antagonism by MRS2500 and BPTU. We had found that in ligand free apo state of $P2Y_1R$ the distance between Asp204 and Arg310 was 2.6 Å and remained stable during the course of simulation (Fig. 3A and B). Binding of polyP-14 and ADP, disrupted the ionic lock of these residues, and led to the step-wise increase of distance between Asp204 and Arg310 up to 5.5 Å (Fig. 3A and B). These observations were also supported by evaluation of electrostatic interactions between these two amino acids (Sup. Fig. 2 D).

In the previous report it was shown that the disruption of the ionic lock between Asp204 and Arg310 in the presence of ADP led to the significant increase of the $P2Y_1R$'s binding pocket size. To assess whether the polyP molecule can also increase the SASA of the receptor's binding pocket, we measured the solvent accessible area of receptor considering the last 100 ns of simulations for all systems. In our simulations, the solvent-accessible surface area (SASA) of the ligand-binding pocket of P2Y1R in the apo state was 160 $Å^2$ after 300 ns of simulation, whereas in the presence of ADP and PolyP-14, this area increased to 175 ± 3 and 174 ± 6 $Å^2$ (Fig. 3C).

3.2. Binding of polyP and ADP to P2Y1R causes formation of continuous water channel inside the $P2Y_1R$ and transmembrane helixes movement

It has been shown that water molecules play significant role in GPCR activation [21]. In our experiments we also observed the continuous water channel formation inside the P2Y1R during our simulations in ADP and PolyP bound states. The ligand binding pocket of $P2Y_1R$ in apo state was filled with water molecules (Fig. 4 A), however the inner part of the receptor next to highly conservative Y324 residue was remaining hydrophobic.

During the course of simulation there were only random penetration of water molecules inside the receptor (Fig. 4 A – water density map, and D). However, in the presence of both polyP-14 and ADP, continuous water channels were formed inside the P2Y1R during the whole course of the simulation (Fig. 4 B, C, D). Interestingly, in our simulations, the binding of polyP-14 to P2Y1R resulted in a greater penetration of water molecules inside the receptor compared to ADP (Fig. 4D and E). Possibly, this effect was associated with a more pronounced shift in RMSD in the presence of polyP compared to the ADP-bound state (Sup. Fig. 2A and B).

Numerous studies indicate that GPCR activation involves significant movement of TM3, TM6, and TM7, forming an intracellular pocket to accommodate downstream transducers [39,40], which was proven to be true for $P2Y_1R$ activation by ADP as well [22,38]. To assess the effect of polyP binding on TM positioning, we sampled the distances between TM3, TM6 and TM7 of $P2Y_1R$ in our systems during the last 100 ns of simulations. We found that the distances between TM helices in apo state of the receptor remains low and don't change much during the course of simulation and the mean distances between selected helices are as follow: d(TM3-TM7), 16.2 ± 0.9 Å; d(TM3-TM6), 10.4 ± 0.4 Å; and d(TM6-TM7), 13.5 ± 0.9 Å. However, in ADP bound state the average distances between selected TM helices drastically increase: d (TM3-TM7), 28.9 ± 2.7 Å; d(TM3-TM6), 13.5 ± 1.5 Å; and d (TM6-TM7), 19.9 ± 3.3 Å. The same manner of conformational changes in TM helices positions we observed for $P2Y_1R$ in PolyP-bound state: d(TM3-TM7), 29.9 ± 1.99 Å; d(TM3-TM6), 14.8 ± 0.7 Å; and d (TM6-TM7), 19.1±2 Å (Fig. 5).

Thus, our observations show that polyP binding to $P2Y_1R$ can lead to the conformational shift of TM helixes in $P2Y_1R$ in highly similar manner compared to ADP. These conformational changes in intracellular TM helices are considered to create a large void, enabling the G-protein binding to activated $P2Y_1R$, which afterwards leads to signal transduction in the cell by G-protein mediated way.

3.3. PolyP-14 has higher binding affinity to $P2Y_1R$ in comparison to ADP

In all our simulations we observed stabilization of $P2Y_1R$ conformational changes in polyP-bound state. Our results showed, that during last 100 ns of simulation, after most conformational changes occurred and receptor transition to active state happened, $P2Y_1R$ in polyP-14 bound state explores less conformational space in comparison to ADP-bound and apo states. We hypothesized that this phenomenon is caused by higher binding energies and as a result higher affinity of PolyP to $P2Y_1R$ in comparison to ADP. The higher affinity leads to better stabilization of the receptor in its conformational state. To prove this idea, we aimed to measure the binding free energies of PolyP-14 and ADP to $P2Y_1R$ by performing Umbrella Sampling (US) simulations (Fig. 6 A).

The resulting PMF curves for both PolyP-14 and ADP represent the binding energies between the ligand and $P2Y_1R$. (Fig. 6 B). We computed the binding energies of ligands to receptors as a minimum point of the PMF curve, which is represented in Fig. 6. Our results show, that PolyP-14 has 5-fold higher binging energy to $P2Y_1$ purinoreceptor in comparison to ADP. These findings prove the ability of PolyP binding to $P2Y_1R$ and its higher affinity towards the receptor in comparison to its native ligand. Moreover, the higher binding energy also can cause higher stabilization effects on activated $P2Y_1R$, which were detected in our simulations.

3.4. PolyP induces calcium signal in skin fibroblasts with same shape and amplitude as ADP

It is well known that platelet derived ADP and polyP induce blood coagulation processes and affect surrounding vascular endothelial cells and skin fibroblasts [41,42]. Activation of the P2Y1R play significant role in ADP and polyP derived effects in vascular endothelial cells and skin fibroblasts [15,41]. Thus, in next series of experiments we used culture of human skin fibroblast to study the difference in PolyP- and ADP-induced calcium signal through the activation of P2Y1 receptors. Application of 50 μM ADP induced peak like increase in cytosolic

[1] The structure with PDB ID 8WJX has been deposited in the Protein Data Bank in 2023 but has not yet been published in a peer-reviewed journal.

Table 2
Interaction of polyP and ADP with $P2Y_1R$ amino acids at the end of the simulation.

Part of the ligand	1st Replica with ADP 300 ns	2nd Replica with ADP 300 ns	3rd Replica with ADP 300 ns	1st Replica with polyP-14 300 ns	2nd Replica with polyP-14 300 ns	3rd Replica with polyP-14 300 ns
Pyrophosphate	Ser205	Asp300	Phe290	Lys196	Arg310	Arg310
	Asp208	Tyr303	Asp208	Arg195	Gln307	Tyr203
	Cys42	Asn299	Arg287	Lys46	Tyr303	Tyr303
		Arg287	Phe40	Arg41	Arg287	Lys46
Purine ring	Arg195	Ser205		Arg310	Tyr203	Lys196
	Leu44	Asp204		Arg128	Arg41	Arg287
	Thr201	Tyr203		Arg287	Phe40	Arg195
		Arg287		Tyr303	Lys196	Arg41
Sugar ring		Cys202	Gln291	Phe40	Arg195	Phe40
		Arg195	Arg287	Tyr203		
		Thr201	Phe40			

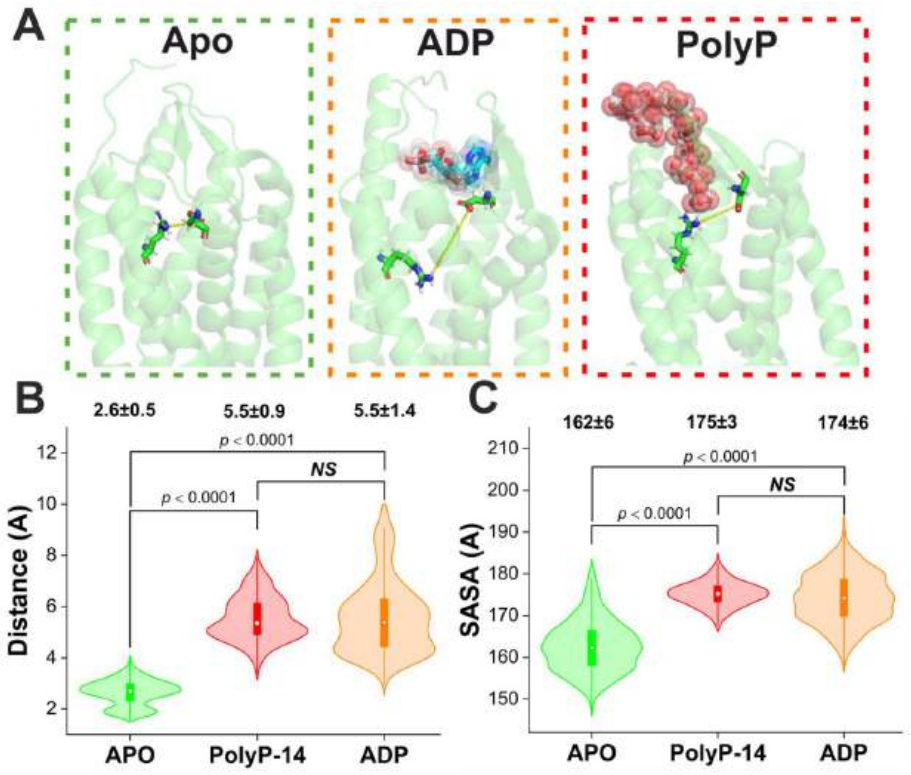

Fig. 3. Binding of polyP and ADP to P2Y1R causes disruption of ionic lock between Asp204 and Arg310 and increase of SASA. A. Positioning of the ASP204 and Arg310 residues in P2Y1R during the last frame of 300 ns simulations. The yellow line represents the distance between amino acids; **B**. A distribution diagram showing the distance between Asp204 and Arg310 residues in P2Y1R during the last 100 ns of simulation; **C**. Total solvent accessible area of $P2Y_1R$ ligand binding pocket during the last 100 ns of simulations. The mean ± sem of the distribution is shown above.

calcium concentration ($[Ca^{2+}]_c$) measured using fura-2 ratio (340nm/380 nm) (Fig. 7A and B). Addition of 50 μM polyP also increased $[Ca^{2+}]_c$ in fibroblasts (red traces, Fig. 7A and B). It should be noted that the amplitude of the calcium signal was not significantly different between polyP and ADP (Fig. 7C) while the recovery (time to return to basal $[Ca^{2+}]_c$) was faster in experiments with polyP (Fig. 7D). Thus, both ADP and polyP are able to induce calcium signal in skin fibroblasts.

4. Discussion

GPCRs remain major drug targets, despite our incomplete understanding of their molecular mechanisms of activation and inhibition. The P2Y family of purinoreceptors are represented by eight members, which are divided into two sub-families based on sequence homology and signaling pathways. These include activating $P2Y_1R$-like receptors that primarily coupled with $G_q/_{11}$ proteins and inhibitory $P2Y_{12}R$-like receptors that activate $G_i/_o$ proteins [23]. Our experiments show that polyP – a molecule composed only from orthophosphate residues, can activate $P2Y_1R$ with the same efficacy as its natural ligand, ADP. Moreover, adenosine is known to be unable to activate P2Y1 receptors, and instead transmitting signals exclusively through its own class of purinergic receptors, the P1 receptors [45]. These findings indicate that the interaction between the pyrophosphate group of ADP or polyphosphate and specific amino acids is a critical step in $P2Y_1R$ activation. This conclusion is strongly supported by experiments involving the caged form of 2-MeSADP - a potent $P2Y_1R$ agonist. Blocking of the β-phosphate group of 2-MeSADP totally abolished its ability to activate $P2Y_1R$ and $P2Y_{12}R$ in astrocytoma cells and human platelets [46]. Moreover, mild irradiation with long-wave UV light (360 nm) restored the agonist's initial structure and ability to activate both receptors [46], further confirming the essential role of the pyrophosphate group in

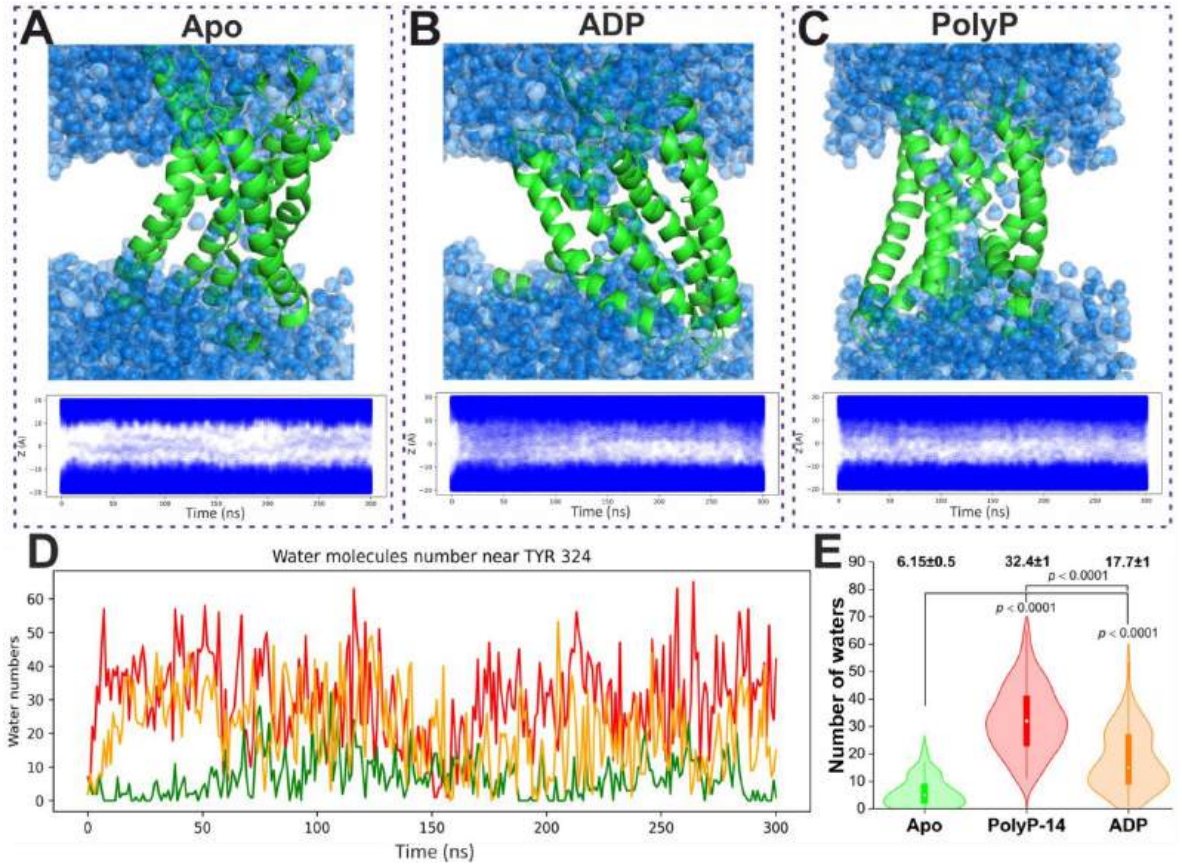

Fig. 4. The formation of continuous water channel inside of $P2Y_1R$ in presence of PolyP-14 and ADP. Representative figures of water channels during the last frame of simulations and water density within $P2Y_1R$ in apo- (**A**), ADP-bound (**B**) and PolyP-14-bound (**C**) states. **D**. The number of water molecules within a 5 Å radius of the conserved Y324 residue throughout the simulation; **E.** A distribution diagram showing the number of water molecules near the conserved Y324 residue during the last 100 ns of the simulations. The mean ± sem of the distribution is shown above.

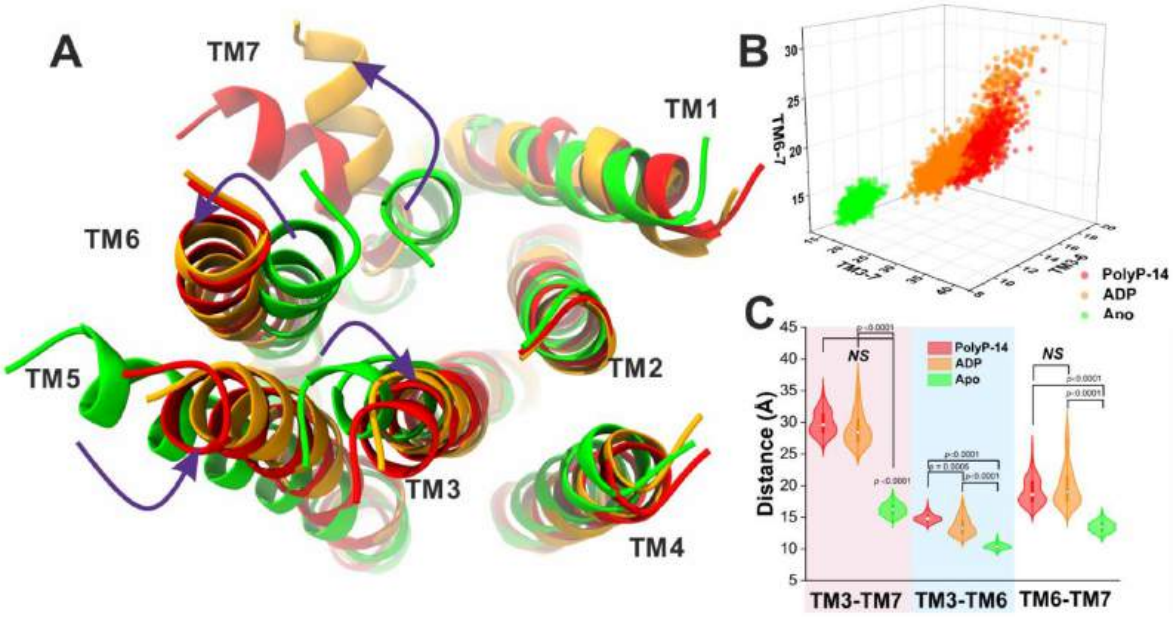

Fig. 5. Helix movements of $P2Y_1R$ in different states. A. View of $P2Y_1R$ helix positions (intracellular loops are not shown) from intracellular side in apo (green), ADP-bound (orange) and polyP-bound (red) states, blue arrows denote the conformational changes of activated $P2Y_1R$. B, C. Distances between TM3, TM6 and TM7 of $P2Y_1R$ during the last 100 ns of MD simulations in different states.

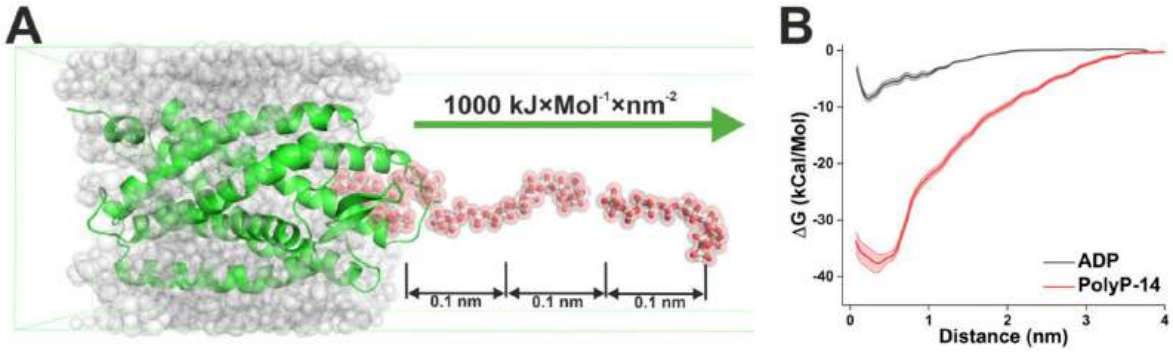

Fig. 6. The Umbrella Sampling simulations. **A**. Scheme, representing the Umbrella Sampling simulation of PolyP-14 along z-axis. **B.** Binding energies of PolyP-14 and ADP to $P2Y_1R$.

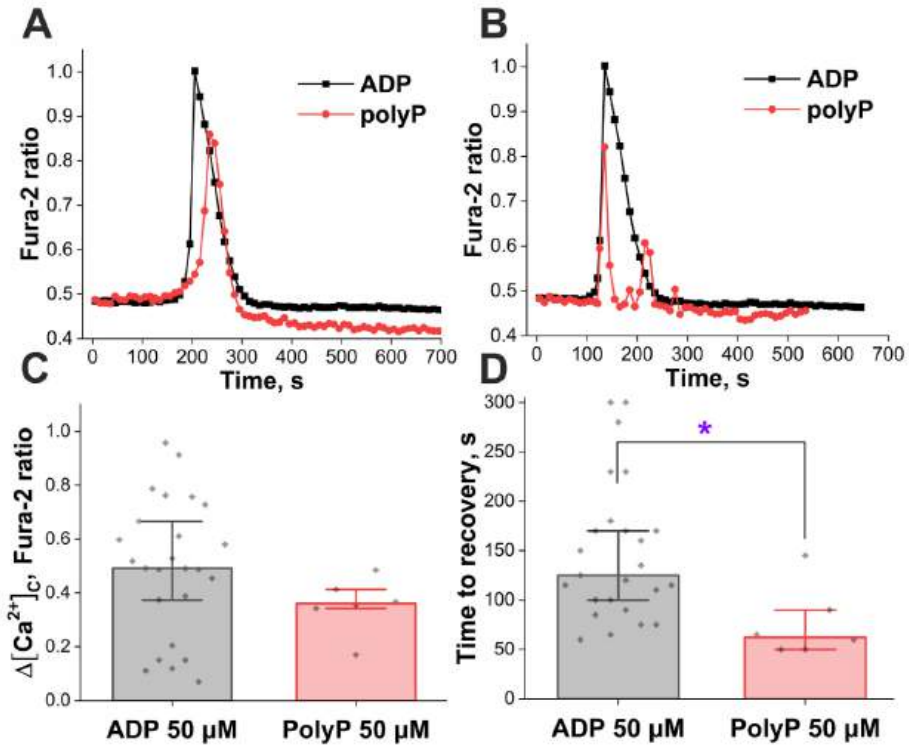

Fig. 7. ADP and polyP induce increase of $[Ca^{2+}]_c$ in skin fibroblasts. A, B – representative traces of fura-2 ratio in skin fibroblasts in response to 50 μM ADP (black trace) or 50 μM polyP (red trace). **C** - amplitude of $[Ca^{2+}]_c$ in fibroblasts measured as Δ fura-2 ratio in response to 50 μM ADP or 50 μM polyP; **D** - Time to recover of $[Ca^{2+}]_c$ in fibroblasts (in sec) to basal level. N = 3; n = 6 for both ADP and polyP (N - number of days, n-number of coverslips). *p < 0.05.

receptor activation.

Although the obtained results suggest such hypotheses, previously published structural data and site-directed mutagenesis studies indicate that mutations in various amino acids - associated with different regions of the ADP molecule - can severely disrupt P2Y1R activation (Sup. Tables 2 and 3). At the same time, multiple studies have demonstrated that certain amino acid residues may interact with both the pyrophosphate moiety of the ligand and its purine or sugar components. This is particularly evident for residues such as Arg287, Tyr203, Tyr303, among others (Sup.Table 2). Moreover, previous studies have shown that even mutations in amino acid residues that do not directly interact with any part of the ADP molecule can significantly impair P2Y1R activation by ADP (Sup. Table 3). Another interesting observation is that, structural studies have shown that many of the P2Y1R's amino acid residues involved in binding ADP or 2MeSADP also participate in interactions with the antagonist MRS2500 (Sup. Tables 2 and 3), however, such interactions do not result in receptor activation. We believe that the application of advanced computational approaches [47], in combination with existing mutational data [23,38,43,44,48], may provide deeper insights into this issue.

Inorganic polyphosphates, due to their highly negative charge, can interact with a wide range of proteins [49]. However, the mechanisms underlying these interactions and their impact on protein functionality remain poorly understood. Recent studies have demonstrated that the binding of polyP to different proteins helps preserve their functionality under cellular stress conditions [50]. Additionally, direct interaction of polyP with amyloids facilitates the formation of mature fibrils and reduces the formation of toxic amyloid oligomers and protofibrils [51,52]. Some cellular effects mediated by extracellular polyP have been shown to depend on the inhibition of receptor for advanced glycation end-products (RAGE) [15–17] and TRPM8 [53]. This suggests that direct interaction between polyP and these receptors may also be possible. We have recently demonstrated that polyphosphates can modulate thymocyte functions through the activation of P2X purinergic receptors [54],

suggesting that these molecules may interact not only with P2Y1R but also with other purinergic receptors, possibly depending on their expression profiles. These findings contribute to a better understanding of previously observed effects of polyphosphates. For instance, during cerebral ischemia–reperfusion, polyP exerted a generally protective effect by activating P2Y1R, which in turn reduced glutamate receptor hyperactivation [14]. However, in another context, polyP released by astrocytes carrying ALS/FTD-associated mutations induced toxicity to neighboring motoneurons [13]. Interestingly, Bertin et al. recently reported a significant increase in surface density and functional activity of P2X4 receptors in neurons, microglia, and peripheral macrophages in the ALS SOD1-G93A model [55], suggesting a potential mechanism for polyP-induced toxicity in ALS.

The main part of our research was made with polyP-14 – the polymer consisted of 14 orthophosphate residues. In mammalian cells the length of polyPs varies up to 100 orthophosphate residues, moreover, the symbiotic bacteria of mammalian organisms contain polyphosphates with polymerization rates up to 1000 residues [56]. While the behavior of P2Y1R in the presence of longer polyP chains could provide a deeper understanding into the activation process, however, such investigations would require significantly greater computational resources.

In our study, we showed for the first time that polyP can activate calcium signalling in skin fibroblasts. Previous reports have indicated that certain effects of polyP, beyond P2Y1R activation, dependent on the activity of calcium channels [57], P2X receptors , RAGE receptors [15] and TRPM8 [53], among others. Moreover, in 2021, it was demonstrated that co-application of Ca^{2+} and polyP facilitates polyP's entry into the cell [57], where it can potentially modulate calcium signaling through TRPA1 [59], TRPM8 [60] or PMCA [61]. Additionally, recent reports have shown that activation of RAGE receptors can trigger the release of other signaling molecules via exocytosis and stimulate calcium signaling [62].

In conclusion, our research provides valuable insights into the mechanisms of P2Y1R activation and identifies polyphosphates as novel natural agonists for P2Y1R, significantly advancing our understanding in this area. However, further research is required to explore the interaction between polyPs and various calcium signaling systems to gain a comprehensive understanding of the signaling pathways mediated by this polymer.

CRediT authorship contribution statement

Khondamir R. Rustamov: Writing – review & editing, Writing – original draft, Visualization, Validation, Methodology, Investigation, Formal analysis, Conceptualization. **Albert R. Makhmudov:** Investigation. **Fozila R. Ikromova:** Investigation, Formal analysis. **Ekaterina A. Vetrova:** Visualization, Investigation, Formal analysis. **Andrey Y. Vinokurov:** Visualization, Investigation, Formal analysis. **Jamoliddin I. Razzokov:** Validation, Methodology, Data curation. **Andrey Y. Abramov:** Writing – review & editing, Writing – original draft, Validation, Supervision, Funding acquisition. **Artyom Y. Baev:** Writing – review & editing, Writing – original draft, Visualization, Supervision, Resources, Project administration, Investigation, Funding acquisition, Formal analysis, Data curation, Conceptualization.

Lead contact

Further information and requests for resources should be directed to and will be fulfilled by the lead contact, Artyom Y. Baev (baev.a.yu@gmail.com).

Materials availability

This study did not generate new unique reagents.

Data and code availability

All original code used in this study has been deposited at GutHub repository and is publicly available at (https://github.com/KhondamirRustamov/Poly-P-in-silico). All data reported in this paper will be shared by the lead contact upon request. Any additional information needed to reanalyze the data reported in this paper is available from the lead contact upon request.

Declaration of interests

The authors declare that they have no competing interests.

Acknowledgements

This research was supported by FZ-20200929214 (A.Y.B.) grant of Agency for Innovative Development under the Ministry of higher education, science and innovation of the Republic of Uzbekistan, calcium signaling part of this research was supported by the Mega Grant 075-15-2025-011 (A.Y.A.), Russian Federation. We thank prof. Toshikazu Shiba for providing polyphosphate samples for this research. A.R.M. acknowledges the receipt of an Erasmus + Scholarship from the EMJMD TCCM program.

Appendix A. Supplementary data

Supplementary data to this article can be found online at https://doi.org/10.1016/j.abb.2025.110555.

Data availability

Data will be made available on request.

References

[1] A.Y. Baev, A.Y. Abramov, Inorganic polyphosphate and F0F1-ATP synthase of Mammalian mitochondria, Prog. Mol. Subcell. Biol. 61 (2022) 1–13.
[2] A.Y. Abramov, C. Fraley, C.T. Diao, R. Winkfein, M.A. Colicos, M.R. Duchen, R. J. French, E. Pavlov, Targeted polyphosphatase expression alters mitochondrial metabolism and inhibits calcium-dependent cell death, Proc. Natl. Acad. Sci. USA 104 (46) (2007) 18091–18096.
[3] E. Pavlov, R. Aschar-Sobbi, M. Campanella, R.J. Turner, M.R. Gomez-Garcia, A. Y. Abramov, Inorganic polyphosphate and energy metabolism in mammalian cells, J. Biol. Chem. 285 (13) (2010) 9420–9428.
[4] A.Y. Baev, P.R. Angelova, A.Y. Abramov, Inorganic polyphosphate is produced and hydrolyzed in F0F1-ATP synthase of mammalian mitochondria, Biochem. J. 477 (8) (2020) 1515–1524.
[5] M.E. Solesio, L. Xie, B. McIntyre, M. Ellenberger, E. Mitaishvili, S. Bhadra-Lobo, L. F. Bettcher, J.N. Bazil, D. Raftery, U. Jakob, E.V. Pavlov, Depletion of mitochondrial inorganic polyphosphate (polyP) in mammalian cells causes metabolic shift from oxidative phosphorylation to glycolysis, Biochem. J. 478 (8) (2021) 1631–1646.
[6] M. Guitart-Mampel, P. Urquiza, F. Carnevale Neto, J.R. Anderson, V. Hambardikar, E.R. Scoma, G.E. Merrihew, L. Wang, M.J. MacCoss, D. Raftery, M.J. Peffers, M. E. Solesio, Mitochondrial inorganic polyphosphate (polyP) is a potent regulator of Mammalian bioenergetics in SH-SY5Y cells: a proteomics and metabolomics study, Front. Cell Dev. Biol. 10 (2022) 833127.
[7] J.H. Morrissey, S.H. Choi, S.A. Smith, Polyphosphate: an ancient molecule that links platelets, coagulation, and inflammation, Blood 119 (25) (2012) 5972–5979.
[8] F. Muller, N.J. Mutch, W.A. Schenk, S.A. Smith, L. Esterl, H.M. Spronk, S. Schmidbauer, W.A. Gahl, J.H. Morrissey, T. Renne, Platelet polyphosphates are proinflammatory and procoagulant mediators in vivo, Cell 139 (6) (2009) 1143–1156.
[9] P.M. Suess, S.A. Smith, J.H. Morrissey, Platelet polyphosphate induces fibroblast chemotaxis and myofibroblast differentiation, J. Thromb. Haemostasis : JTH 18 (11) (2020) 3043–3052.
[10] K.M. Holmstrom, N. Marina, A.Y. Baev, N.W. Wood, A.V. Gourine, A.Y. Abramov, Signalling properties of inorganic polyphosphate in the mammalian brain, Nat. Commun. 4 (2013) 1362.
[11] P.R. Angelova, A.Y. Baev, A.V. Berezhnov, A.Y. Abramov, Role of inorganic polyphosphate in mammalian cells: from signal transduction and mitochondrial metabolism to cell death, Biochem. Soc. Trans. 44 (1) (2016) 40–45.
[12] P.R. Angelova, K.Z. Iversen, A.G. Teschemacher, S. Kasparov, A.V. Gourine, A. Y. Abramov, Signal transduction in astrocytes: localization and release of inorganic polyphosphate, Glia 66 (10) (2018) 2126–2136.

[13] C. Arredondo, C. Cefaliello, A. Dyrda, N. Jury, P. Martinez, I. Díaz, A. Amaro, H. Tran, D. Morales, M. Pertusa, L. Stoica, E. Fritz, D. Corvalán, S. Abarzúa, M. Méndez-Ruette, P. Fernández, F. Rojas, M.S. Kumar, R. Aguilar, S. Almeida, A. Weiss, F.J. Bustos, F. González-Nilo, C. Otero, M.F. Tevy, D.A. Bosco, J.C. Sáez, T. Kähne, F.-B. Gao, J.D. Berry, K. Nicholson, M. Sena-Esteves, R. Madrid, D. Varela, M. Montecino, R.H. Brown, B. van Zundert, Excessive release of inorganic polyphosphate by ALS/FTD astrocytes causes non-cell-autonomous toxicity to motoneurons, Neuron 110 (10) (2022) 1656–1670.e12.
[14] M. Maiolino, N. O'Neill, V. Lariccia, S. Amoroso, S. Sylantyev, P.R. Angelova, A. Y. Abramov, Inorganic polyphosphate regulates AMPA and NMDA receptors and protects against glutamate excitotoxicity via activation of P2Y receptors, J. Neurosci. : off. J Soc. Neurosci. 39 (31) (2019) 6038–6048.
[15] P. Dinarvand, S.M. Hassanian, S.H. Qureshi, C. Manithody, J.C. Eissenberg, L. Yang, A.R. Rezaie, Polyphosphate amplifies proinflammatory responses of nuclear proteins through interaction with receptor for advanced glycation end products and P2Y1 purinergic receptor, Blood 123 (6) (2014) 935–945.
[16] S.M. Hassanian, P. Dinarvand, S.A. Smith, A.R. Rezaie, Inorganic polyphosphate elicits pro-inflammatory responses through activation of the mammalian target of rapamycin complexes 1 and 2 in vascular endothelial cells, J. Thromb. Haemostasis : JTH 13 (5) (2015) 860–871.
[17] S.M. Hassanian, A. Ardeshirylajimi, P. Dinarvand, A.R. Rezaie, Inorganic polyphosphate promotes cyclin D1 synthesis through activation of mTOR/Wnt/beta-catenin signaling in endothelial cells, J. Thromb. Haemostasis : JTH 14 (11) (2016) 2261–2273.
[18] W.E. Muller, E. Tolba, Q. Feng, H.C. Schroder, J.S. Markl, M. Kokkinopoulou, X. Wang, Amorphous Ca(2)(+) polyphosphate nanoparticles regulate the ATP level in bone-like SaOS-2 cells, J. Cell Sci. 128 (11) (2015) 2202–2207.
[19] W.E.G. Muller, S. Wang, M. Neufurth, M. Kokkinopoulou, Q. Feng, H.C. Schroder, X. Wang, Polyphosphate as a donor of high-energy phosphate for the synthesis of ADP and ATP, J. Cell Sci. 130 (16) (2017) 2747–2756.
[20] G.G. Yegutkin, Adenosine metabolism in the vascular system, Biochem. Pharmacol. 187 (2021) 114373.
[21] S. Yuan, S. Filipek, K. Palczewski, H. Vogel, Activation of G-protein-coupled receptors correlates with the formation of a continuous internal water pathway, Nat. Commun. 5 (2014) 4733.
[22] S. Yuan, H.C. Chan, H. Vogel, S. Filipek, R.C. Stevens, K. Palczewski, The molecular mechanism of P2Y1 receptor activation, Angew. Chem. 55 (35) (2016) 10331–10335.
[23] D. Zhang, Z.G. Gao, K. Zhang, E. Kiselev, S. Crane, J. Wang, S. Paoletta, C. Yi, L. Ma, W. Zhang, G.W. Han, H. Liu, V. Cherezov, V. Katritch, H. Jiang, R.C. Stevens, K.A. Jacobson, Q. Zhao, B. Wu, Two disparate ligand-binding sites in the human P2Y1 receptor, Nature 520 (7547) (2015) 317–321.
[24] E. Chun, A.A. Thompson, W. Liu, C.B. Roth, M.T. Griffith, V. Katritch, J. Kunken, F. Xu, V. Cherezov, M.A. Hanson, R.C. Stevens, Fusion partner toolchest for the stabilization and crystallization of G protein-coupled receptors, Structure 20 (6) (2012) 967–976.
[25] J. Jumper, R. Evans, A. Pritzel, T. Green, M. Figurnov, O. Ronneberger, K. Tunyasuvunakool, R. Bates, A. Žídek, A.J.N. Potapenko, Highly accurate protein structure prediction with AlphaFold 596 (7873) (2021) 583–589.
[26] J.P. Roney, S.J.P.R.L. Ovchinnikov, State-of-the-art estimation of protein model accuracy using AlphaFold 129 (23) (2022) 238101.
[27] I. Igashov, H. Stärk, C. Vignac, A. Schneuing, V.G. Satorras, P. Frossard, M. Welling, M. Bronstein, B.J.N.M.I. Correia, Equivariant 3D-conditional Diffusion Model for Molecular Linker Design, 2024, pp. 1–11.
[28] S. Forli, R. Huey, M.E. Pique, M.F. Sanner, D.S. Goodsell, A.J. Olson, Computational protein-ligand docking and virtual drug screening with the AutoDock suite, Nat. Protoc. 11 (5) (2016) 905–919.
[29] H. Guterres, S.J. Park, H. Zhang, T. Perone, J. Kim, W.J.P.S. Im, CHARMM-GUI high-throughput simulator for efficient evaluation of protein–ligand interactions with different force fields 31 (9) (2022) e4413.
[30] M.J. Abraham, T. Murtola, R. Schulz, S. Páll, J.C. Smith, B. Hess, E.J.S. Lindahl, GROMACS: High Performance Molecular Simulations Through multi-level Parallelism from Laptops to Supercomputers, vol. 1, 2015, pp. 19–25.
[31] J. Huang, S. Rauscher, G. Nawrocki, T. Ran, M. Feig, B.L. De Groot, H. Grubmüller, A.D.J.N.m. MacKerell Jr., CHARMM36m: an improved force field for folded and intrinsically disordered proteins 14 (1) (2017) 71–73.
[32] K.R. Rustamov, A.Y. Baev, MSA clustering enhances AF-Multimer's ability to predict conformational landscapes of protein–protein interactions, Bioinform. Adv. 5 (1) (2024).
[33] J. Razzokov, S. Fazliev, M. Makhkamov, P. Marimuthu, A. Baev, E. Kurganov, Effect of electric field on alpha-Synuclein fibrils: revealed by molecular dynamics simulations, Int. J. Mol. Sci. 24 (7) (2023).
[34] M. Makhkamov, A. Baev, E. Kurganov, J. Razzokov, Understanding Osaka mutation polymorphic Abeta fibril response to static and oscillating electric fields: insights from computational modeling, Sci. Rep. 14 (1) (2024) 22246.
[35] K. Rustamov, K. Nebesnaya, A.Y. Baev, Computational design of novel ampar and nmdar peptide modulators, in: ICLR 2024 Workshop on Generative and Experimental Perspectives for Biomolecular Design, 2024.
[36] A.Y. Vinokurov, A.A. Palalov, K.A. Kritskaya, S.V. Demyanenko, D.G. Garbuz, M. B. Evgen'ev, N. Esteras, A.Y. Abramov, Cell-permeable HSP70 protects neurons and astrocytes against cell death in the rotenone-induced and familial models of Parkinson's disease, Mol. Neurobiol. 61 (10) (2024) 7785–7795.
[37] A. Ciancetta, R.D. O'Connor, S. Paoletta, K.A. Jacobson, Demystifying P2Y(1) receptor ligand recognition through docking and molecular dynamics analyses, J. Chem. Inf. Model. 57 (12) (2017) 3104–3123.
[38] B. Li, S. Han, M. Wang, Y. Yu, L. Ma, X. Chu, Q. Tan, Q. Zhao, B. Wu, Structural insights into signal transduction of the purinergic receptors P2Y1R and P2Y12R, Protein Cell 14 (5) (2023) 382–386.
[39] A. Mafi, S.K. Kim, W.A. Goddard, 3rd, the mechanism for ligand activation of the GPCR-G protein complex, Proc. Natl. Acad. Sci. USA 119 (18) (2022) e2110085119.
[40] A. Manglik, A.C. Kruse, Structural basis for G protein-coupled receptor activation, Biochemistry 56 (42) (2017) 5628–5634.
[41] P.A. Borges, I. Waclawiak, J.L. Georgii, V.D.S. Fraga-Junior, J.F. Barros, F. S. Lemos, T. Russo-Abrahao, E.M. Saraiva, C.M. Takiya, R. Coutinho-Silva, C. Penido, C. Mermelstein, J.R. Meyer-Fernandes, F.B. Canto, J.S. Neves, P.A. Melo, C. Canetti, C.F. Benjamim, Adenosine diphosphate improves wound healing in diabetic mice through P2Y(12) receptor activation, Front. Immunol. 12 (2021) 651740.
[42] B.C. Carney, C.M. Simbulan-Rosenthal, A. Gaur, B.J. Browne, M. Moghe, E. Crooke, L.T. Moffatt, J.W. Shupp, D.S. Rosenthal, Inorganic polyphosphate in platelet rich plasma accelerates re-epithelialization in vitro and in vivo, Regen. Ther. 15 (2020) 138–148.
[43] C. Hoffmann, S. Moro, R.A. Nicholas, T.K. Harden, K.A. Jacobson, The role of amino acids in extracellular loops of the human P2Y1 receptor in surface expression and activation processes, J. Biol. Chem. 274 (21) (1999) 14639–14647.
[44] S. Moro, C. Hoffmann, K.A. Jacobson, Role of the extracellular loops of G protein-coupled receptors in ligand recognition: a molecular modeling study of the human P2Y1 receptor, Biochemistry 38 (12) (1999) 3498–3507.
[45] Z. Huang, N. Xie, P. Illes, F. Di Virgilio, H. Ulrich, A. Semyanov, A. Verkhratsky, B. Sperlagh, S.G. Yu, C. Huang, Y. Tang, From purines to purinergic signalling: molecular functions and human diseases, Signal Transduct. Targeted Ther. 6 (1) (2021) 162.
[46] Z.G. Gao, B. Hechler, P. Besada, C. Gachet, K.A. Jacobson, Caged agonist of P2Y1 and P2Y12 receptors for light-directed facilitation of platelet aggregation, Biochem. Pharmacol. 75 (6) (2008) 1341–1347.
[47] K.R. Rustamov, J.I. Razzokov, A.Y. Baev, Investigation of structural mechanisms underlying p53 dysfunction caused by 148 missense mutations using AlphaFold3 and molecular dynamics simulations, J. Chem. Inf. Model. 65 (12) (2025) 6322–6330.
[48] S. Moro, D. Guo, E. Camaioni, J.L. Boyer, T.K. Harden, K.A. Jacobson, Human P2Y1 receptor: molecular modeling and site-directed mutagenesis as tools to identify agonist and antagonist recognition sites, J. Med. Chem. 41 (9) (1998) 1456–1466.
[49] R.S. Negreiros, N. Lander, G. Huang, C.D. Cordeiro, S.A. Smith, J.H. Morrissey, R. Docampo, Inorganic polyphosphate interacts with nucleolar and glycosomal proteins in trypanosomatids, Mol. Microbiol. 110 (6) (2018) 973–994.
[50] M.J. Gray, W.Y. Wholey, N.O. Wagner, C.M. Cremers, A. Mueller-Schickert, N. T. Hock, A.G. Krieger, E.M. Smith, R.A. Bender, J.C. Bardwell, U. Jakob, Polyphosphate is a primordial chaperone, Mol. Cell 53 (5) (2014) 689–699.
[51] C.M. Cremers, D. Knoefler, S. Gates, N. Martin, J.U. Dahl, J. Lempart, L. Xie, M. R. Chapman, V. Galvan, D.R. Southworth, U. Jakob, Polyphosphate: a conserved modifier of amyloidogenic processes, Mol. Cell 63 (5) (2016) 768–780.
[52] P. Huettemann, P. Mahadevan, J. Lempart, E. Tse, B. Dehury, B.F.P. Edwards, D. R. Southworth, B.R. Sahoo, U. Jakob, Amyloid accelerator polyphosphate fits as the mystery density in alpha-synuclein fibrils, PLoS Biol. 22 (10) (2024) e3002650.
[53] V. Arrè, F. Balestra, R. Scialpi, F. Dituri, R. Donghia, S. Coletta, D. Stabile, A. Bianco, L. Vincenti, S. Fedele, C. Shen, G. Pettinato, M.P. Scavo, G. Giannelli, R. Negro, Inorganic polyphosphate promotes colorectal cancer growth via TRPM8 receptor signaling pathway 16 (19) (2024) 3326.
[54] K.S. Nebesnaya, A.R. Makhmudov, K.R. Rustamov, N.S.H. Rakhmatullina, S. I. Rustamova, U.Z. Mirkhodjaev, O.S. Charishnikova, R.Z. Sabirov, A.Y. Baev, Inorganic polyphosphate regulates functions of thymocytes via activation of P2X purinoreceptors, Biochim. Biophys. Acta Gen. Subj. 1868 (1) (2024) 130523.
[55] E. Bertin, A. Martinez, A. Fayoux, K. Carvalho, S. Carracedo, P.O. Fernagut, F. Koch-Nolte, D. Blum, S.S. Bertrand, E. Boue-Grabot, Increased surface P2X4 receptors by mutant SOD1 proteins contribute to ALS pathogenesis in SOD1-G93A mice, Cell. Mol. Life Sci. 79 (8) (2022) 431.
[56] J. Roewe, G. Stavrides, M. Strueve, A. Sharma, F. Marini, A. Mann, S.A. Smith, Z. Kaya, B. Strobl, M. Mueller, C. Reinhardt, J.H. Morrissey, M. Bosmann, Bacterial polyphosphates interfere with the innate host defense to infection, Nat. Commun. 11 (1) (2020) 4035.
[57] R. Gawri, R. Bielecki, E.W. Salter, A. Zelinka, T. Shiba, G. Collingridge, A. Nagy, R. A. Kandel, The anabolic effect of inorganic polyphosphate on chondrocytes is mediated by calcium signalling, J. Orthop. Res. (2021).
[59] D. Kim, E.J. Cavanaugh, Requirement of a soluble intracellular factor for activation of transient receptor potential A1 by pungent chemicals: role of inorganic polyphosphates, J. Neurosci. : off. J Soc. Neurosci. 27 (24) (2007) 6500–6509.
[60] E. Zakharian, B. Thyagarajan, R.J. French, E. Pavlov, T. Rohacs, Inorganic polyphosphate modulates TRPM8 channels, PLoS One 4 (4) (2009) e5404.
[61] R.N. Reusch, R. Huang, D. Kosk-Kosicka, Novel components and enzymatic activities of the human erythrocyte plasma membrane calcium pump, FEBS Lett. 412 (3) (1997) 592–596.
[62] A. Kamynina, N. Esteras, D.O. Koroev, P.R. Angelova, O.M. Volpina, A.Y. Abramov, Activation of RAGE leads to the release of glutamate from astrocytes and stimulates calcium signal in neurons, J. Cell. Physiol. 236 (9) (2021) 6496–6506.